Scalable Transmission over Heterogenous Networks

Liang Wu*, Yi Zhong*, Wenyi Zhang*, Martin Haenggi†
University of Science and Technology of China*, University of Notre Dame†
{tuohai, geners}@mail.ustc.edu.cn, wenyizha@ustc.edu.cn, mhaenggi@nd.edu

***Abstract*—Transmission of layered source information, such as scalable video coding (SVC), over heterogenous wireless networks is considered in this work. Scalable transmission enables dynamic adaption of source information to the condition of user equipments, and thus is suitable for heterogenous networks in which the transmission link quality varies substantially. Leveraging tools in stochastic geometry, a comprehensive analysis is conducted for several different transmission protocols, focusing on two key performance metrics, Standard-Definition outage probability and High-Definition probability. The proposed transmission protocols are compared in different aspects, and the benefit of interference cancellation is shown to be significant.**

I. Introduction

A. Motivation

The advent of mobile communication and computing keeps driving the data traffic to grow explosively, among which a substantial portion is attributed to multimedia such as mobile video. According to the Cisco Visual Networking Index, mobile video will grow at a compound average growth rate of 69% until 2018, and within the 15.9 exabytes data per month in mobile network by 2018, 11 exabytes will be video related, such as video on demand, video conferencing, and so on. With the release of different types of user equipments (UEs), the requirements on data rate of video transmission vary in a large range.

Advanced source coding techniques, such as scalable video coding (SVC), provide a new dimension of dynamically provisioning wireless resources for the varying requirement and the varying link condition of UEs. SVC is an extension of the H.264/MPEG-4 AVC video compression standard [1], in which the bitstream is encoded into multiple layers, namely a base layer and at least one enhancement layer. The quality of reconstructed video depends on the number of layers decoded and stays the same until a higher enhancement layer is successfully decoded. The number of layers and their code rates may be determined by the requirement and the link condition of the subscribing UE.

On the other hand, cellular networks are evolving from a homogenous architecture to a composition of heterogenous networks, comprised of various types of base stations (BSs) [2]. Each type of BSs has its characteristic transmit power and deployment intensity: for example, macro BSs (MBSs) have larger transmit power, aiming at providing global coverage; femtocell access points (FAPs) are small BSs targeted for home or small business usages. As the distance between a UE and its serving FAP is small, the UE enjoys high quality link and thus power savings. Furthermore, the reduced transmission range also enhances spatial reuse and reduces multiuser interference.

Therefore, when putting together the above two paradigm shifts, namely, shifting from a single-layer video to SVC with multiple layers, and shifting from a single-tier cellular network to heterogenous cellular networks (HCNs) with multiple tiers, it is intuitively apparent that these two technologies would bring about a natural matching between each other. The macro cells aim at providing global coverage and therefore are suitable for supporting the base layer video for a majority of UEs; the small cells (e.g., femto cells) aim at providing small-area high-rate service enhancement for hot spots and therefore are suitable for supporting the enhancement layer video for those UEs subscribing to their services in their vicinity. In this paper, we thus study the problem of scalable transmission over heterogenous networks.

B. Related Work

Despite of their common nature of handling and exploiting heterogeneity, there are only few existing works that consider scalable transmission over heterogenous wireless networks, and these prior works are mainly based on numerical studies of ad hoc algorithms. In [3] an overview of SVC and its relationship to mobile content delivery were discussed focusing on the challenges from time-varying characteristics of mobile communication channels, but the analysis was limited, and HCN was not even existent at that time. In [4], real time use cases of mobile video streaming were presented, for which a variety of parameters like throughput, packet loss ratio, delay, and delay jitter were compared with H.264 single layer video for unicast and multicast scenarios under different degrees of scalability. In [5], the proposed scheme employed WiFi: the base layer was always transmitted over a reliable network such as cellular, whereas the enhancement layer was opportunistically transmitted when additional capacity became available through WiFi. Technical issues associated with the simultaneous use of multiple networks were then discussed. In [6], HCNs with storage-capable small-cell BSs were studied: versions and layers of video have different impacts on the delay-servicing cost tradeoff, depending on the user demand diversity and the network load.

C. Our Work

In this work, we focus on an analytical performance assessment of transmission of layered source information, such as SVC, over tiered HCNs. We consider two-tier HCNs, with one tier being macro cells providing global coverage, and the other tier being femto cells providing hot spot service enhancement. Our model and analysis employ tools from stochastic geometry, which has been extensively used in wireless networks recently; see, e.g., [7].

We propose protocols that enable scalable transmission over a two-tier HCN. For a UE not served by an FAP, its base layer content is transmitted from an MBS. For a UE inside the coverage of, and served by, an FAP, its base layer content is either transmitted from an MBS or from the covering FAP, depending on the protocol used, whereas its enhancement layer content is transmitted from the covering FAP. Both orthogonal and non-orthogonal spectrum allocation schemes are considered; furthermore, for non-orthogonal spectrum allocation, an enhancement based on cancelling the dominant cross-tier interference is proposed and analyzed, which exhibits a substantial performance improvement compared with treating interference as noise. In our analysis, invoking an approximation of the statistics of the Poisson Voronoi cell area, the impact of system load, in terms of the UE density, on the performance is also investigated. The considered key performance metrics are the Standard-Definition outage probability, which is the probability that a UE cannot even successfully decode the base layer content and thus is in an outage state, and the High-Definition probability, which is the probability that a UE inside the coverage of some FAP can successfully decode both the base layer and the enhancement layer contents.

The remaining part of this paper is organized as follows. Section II describes the system model, including the transmission protocols and spectrum allocation schemes. Section III derives the distributions of the number of UEs per cell, sub-band occupancy probabilities, and coverage probabilities. Section IV employs the results obtained in Section III to evaluate the performance metrics, namely the Standard-Definition outage probability and the High-Definition probability. Section V describes and analyzes the improved transmission protocol aided by interference cancellation. Section VI presents numerical results and related discussions. Finally Section VII concludes this paper.

II. System Model

A. Network Model

We consider two-layer SVC, consisting of a base layer and an enhancement layer, whose required data rates are R_{B} and R_{E}, respectively.

We consider a two-tier HCN which consists of two types of BSs, i.e., MBSs and FAPs. These two types of BSs are modeled by two independent Poisson point processes (PPP) Φ_{m} and Φ_{f}, whose intensities are $\lambda_{\mathrm{m}}^{\mathrm{BS}}$ and $\lambda_{\mathrm{f}}^{\mathrm{BS}}$, respectively. Suppose that there exist N sub-bands each of bandwidth W. The transmit powers of an MBS and an FAP over each sub-band are set as P_{m} and P_{f}, respectively. The path loss model is $r^{-\alpha}$,[1] and the small-scale fading distribution is exponential with mean $\mu = 1$ in squared magnitude, i.e., Rayleigh fading. The fading is assumed to be frequency-flat within each sub-band and independent among different sub-bands. We denote the noise variance at each UE by σ^2. When a UE attempts to access the macro tier network, it connects to the MBS, which induces (along with other MBSs in Φ_{m}) the Voronoi cell in which the UE is situated. FAPs aim at providing network access to UEs in their vicinity, and we assume that all FAPs have the same coverage radius R_{f}.

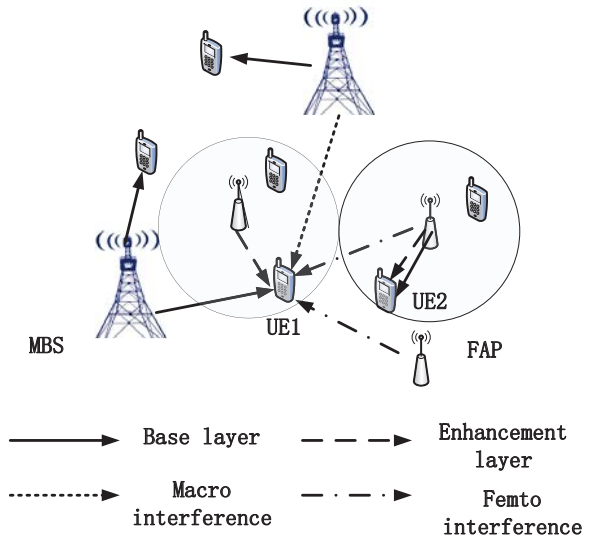

Fig. 1. Illustration of system model. There are two cases for a femto UE to receive its signal: UE1 obtains the base layer from MBS and obtains the enhancement layer from FAP; UE2 obtains both the base layer and the enhancement layer from FAP.

The UEs are divided into two categories, i.e., macro UEs and femto UEs. The locations of macro UEs form a PPP with intensity $\lambda_{\mathrm{m}}^{\mathrm{UE}}$ on the whole plane, while the locations of femto UEs form a Matern cluster process [7] with parent process Φ_{f}–the FAPs–and each cluster forms a PPP of intensity $\lambda_{\mathrm{f}}^{\mathrm{UE}}$ on the disk of radius R_{f}, which implies that the mean number of users per cluster is $\bar{U}_{\mathrm{f}} = \lambda_{\mathrm{f}}^{\mathrm{UE}} \pi R_{\mathrm{f}}^2$. Each femto UE connects to the FAP at its parent point. Several remarks are in order: first, although the coverage regions of two nearby FAPs may overlap and then some UEs may be covered by more than one FAPs, a femto UE always connects to its parent FAP; second, a macro UE can only connect to its serving MBS, even if it is situated within the coverage of an FAP;[2] third, when a femto UE connects to an MBS, it chooses the MBS closest to its parent FAP.

B. Transmission Protocols

Macro UEs attempt to obtain their base layer contents from their serving MBSs and forego the enhancement layer. Femto UEs attempt to obtain their enhancement layer contents from their serving FAPs, and they attempt to obtain their base layer contents either from their serving MBSs with probability p or from their serving FAPs with probability $1-p$. Depending upon the choice of p, we have the following three protocols.

1) Decoupled Transmission: This corresponds to $p = 0$. For a femto UE, both the base layer and the enhancement layer are transmitted from its serving FAP. This protocol thus completely

[1]Here for simplicity we assume the path loss exponent to be the same for MBS and FAP and ignore the effect of shadowing; the extended case of heterogenous path loss exponents and shadowing can be similarly treated following our analytical approach, but with more tedious derivations.

[2]This corresponds to a closed-access femto network, in which only subscribers are allowed to be served by an FAP.

"decouples" the macro tier with its associated macro UEs and the femto tier with its associated femto UEs. It makes full use of the high quality links provided by the femto tier to provide enhancement layer contents.

2) Coupled Transmission: This corresponds to $p = 1$. For a femto UE, its base layer is transmitted from its serving MBS, and its enhancement layer is transmitted from its serving FAP. This protocol is suitable for UEs handed over into the coverage of an FAP, since it enables uninterrupted reception of the base layer from the macro tier and opportunistic reception of the enhancement layer when covered by an FAP.

3) Hybrid Transmission: This corresponds to the general case of $0 < p < 1$. This protocol enables a flexible tradeoff between decoupled transmission and coupled transmission.

C. Spectrum Allocation Schemes

Let $N_{\rm m}$ sub-bands be allocated to macro tier and $N_{\rm f}$ sub-bands to femto tier. Each UE requires one sub-band for each connection. We consider the following two spectrum allocation schemes.

1) Orthogonal: The total N sub-bands are divided into two parts $N = N_{\rm m} + N_{\rm f}$, in which the $N_{\rm m}$ sub-bands used by all the MBSs of the macro tier are orthogonal to those $N_{\rm f}$ sub-bands used by all the FAPs of the femto tier. So there is no inter-tier interference.

2) Non-orthogonal: Compared with the orthogonal case, the two sets of sub-bands may overlap: Each MBS (resp. FAP) independently randomly selects $N_{\rm m}$ (resp. $N_{\rm f}$) sub-bands from the total N sub-bands. The values of $N_{\rm m}$ and $N_{\rm f}$ can be chosen from 1 to N flexibly. So there is inter-tier interference.

III. UE Load, Sub-band Occupancy, and Coverage Probability

This section establishes several auxiliary results for our derivation of the key performance metrics in the next section. We first provide an approximate characterization of the distribution of the number of UEs connected to an MBS or an FAP and then obtain the probability of a sub-band being occupied. The coverage probability is subsequently derived, which is further related to the achievable data rate.

A. UE Load

The number of UEs connected to an MBS or an FAP is determined by the coverage area and the transmission protocol chosen. Denote $U_{\rm m}$ (resp. $U_{\rm f}$) as the number of UEs connected to an MBS (resp. FAP).

1) Decoupled Transmission: MBSs and FAPs serve their own UEs separately. Since the distribution of femto UEs in an FAP coverage disk is a PPP with intensity $\lambda_{\rm f}^{\rm UE}$, the number of femto UEs connected to an FAP is a Poisson random variable (r.v.) with mean $\bar{U}_{\rm f}$, i.e.,

$$\mathbb{P}\{U_{\rm f} = i\} = \frac{(\bar{U}_{\rm f})^i}{i!} e^{-\bar{U}_{\rm f}}, \quad i = 0, 1, \cdots. \tag{1}$$

An MBS covers its Voronoi cell. Denote the area of a Voronoi cell by S. Conditioned on S, the number of macro UEs connected to an MBS, $U_{\rm m}$, is a Poisson r.v. with mean $\lambda_{\rm m}^{\rm UE} S$. There is no known closed form expression of the probability density function (pdf) of the Poisson Voronoi cell area S, but the following approximation [8]

$$f_S(x) \approx \frac{(\lambda_{\rm m}^{\rm BS} c)^c}{\Gamma(c)} x^{c-1} e^{-c\lambda_{\rm m}^{\rm BS} x} \tag{2}$$

has been known to be handy and sufficiently accurate (see, e.g., [9]), where $c = \frac{7}{2}$.

Aided by this approximation, with some manipulations the probability generating function (pgf) of $U_{\rm m}$ is

$$G_{\rm m}(z) = c^c \left(c - \frac{\lambda_{\rm m}^{\rm UE}}{\lambda_{\rm m}^{\rm BS}} (z-1) \right)^{-c}, \tag{3}$$

and the distribution of $U_{\rm m}$ follows as

$$\mathbb{P}\{U_{\rm m} = i\} = \frac{G_{\rm m}^{(i)}(0)}{i!}, i = 0, 1, \cdots. \tag{4}$$

2) Coupled Transmission: The distribution of femto UEs inside the coverage of an FAP is the same as that in *Decoupled Transmission*. An MBS not only serves the macro UEs situated in its Voronoi cell, but also serves the femto UEs belonging to the FAPs in this Voronoi cell. We denote the number of the macro UEs as $U_{\rm MBS}$, which can be characterized by (4), and the total number of the served femto UEs as $U_{\rm FAP}$, which is given by $U_{\rm FAP} = \sum_{i=1}^{N_{\rm c}} N_{{\rm f},i}$, where $N_{\rm c}$ denotes the number of FAPs covered in the Voronoi cell and $N_{{\rm f},i}$ denotes the number of femto UEs belonging to the ith FAP. The total number of UEs served by an MBS is thus

$$U_{\rm m} = U_{\rm MBS} + U_{\rm FAP}. \tag{5}$$

Since $U_{\rm MBS}$ is independent of $U_{\rm FAP}$, the pgf of $U_{\rm m}$, denoted by $G_{\rm m}(z)$, is

$$G_{\rm m}(z) = G_{\rm MBS}(z) G_{\rm FAP}(z), \tag{6}$$

where $G_{\rm MBS}(z)$ (resp. $G_{\rm FAP}(z)$) is the pgf of $U_{\rm MBS}$ (resp. $U_{\rm FAP}$).

Conditioned on the Voronoi cell area S, the conditional pgf of $U_{\rm MBS}$ is

$$G_{\rm MBS}(z|S) = e^{\lambda_{\rm m}^{\rm UE} S(z-1)}; \tag{7}$$

since $U_{\rm FAP}$ is a compound Poisson r.v., its conditional pgf is

$$G_{\rm FAP}(z|S) = e^{\lambda_{\rm f}^{\rm BS} S(e^{\bar{U}_{\rm f}(z-1)} - 1)}. \tag{8}$$

Marginalizing with S, we get the pgf of $U_{\rm m}$ as

$$G_{\rm m}(z) = c^c \Big(c - \frac{\lambda_{\rm m}^{\rm UE}}{\lambda_{\rm m}^{\rm BS}} (z-1) + \frac{\lambda_{\rm f}^{\rm BS}}{\lambda_{\rm m}^{\rm BS}} (1 - e^{\bar{U}_{\rm f}(z-1)}) \Big)^{-c}, \tag{9}$$

and the distribution of $U_{\rm m}$ follows.

3) Hybrid Transmission: The analysis is similar to that for *Coupled Transmission*. The only difference is that since a femto UE attempts to connect to its serving MBS with probability p, there is a thinning effect, due to which the expression of $G_{\rm m}(z)$ in (9) is replaced by

$$c^c \Big(c - \frac{\lambda_{\rm m}^{\rm UE}}{\lambda_{\rm m}^{\rm BS}} (z-1) + \frac{\lambda_{\rm f}^{\rm BS}}{\lambda_{\rm m}^{\rm BS}} (1 - e^{p\bar{U}_{\rm f}(z-1)}) \Big)^{-c}. \tag{10}$$

B. Sub-band Occupancy

1) Orthogonal Spectrum Allocation: The probability that a sub-band is used by an MBS is

$$P_{\text{busy}}^{\text{m},\perp} = \frac{1}{N_{\text{m}}} \sum_{i=0}^{\infty} \min\{i, N_{\text{m}}\} \mathbb{P}\{U_{\text{m}} = i\}, \tag{11}$$

and the probability that a sub-band is used by an FAP is

$$P_{\text{busy}}^{\text{f},\perp} = \frac{1}{N_{\text{f}}} \sum_{i=0}^{\infty} \min\{i, N_{\text{f}}\} \mathbb{P}\{U_{\text{f}} = i\}. \tag{12}$$

2) Non-orthogonal Spectrum Allocation: For the non-orthogonal case, both MBS and FAP choose a sub-band randomly from N bands, so the probability that a sub-band is used by an MBS is

$$P_{\text{busy}}^{\text{m},\not\perp} = \frac{1}{N} \sum_{i=0}^{\infty} \min\{i, N_{\text{m}}\} \mathbb{P}\{U_{\text{m}} = i\}, \tag{13}$$

and the probability that a sub-band is used by an FAP is

$$P_{\text{busy}}^{\text{f},\not\perp} = \frac{1}{N} \sum_{i=0}^{\infty} \min\{i, N_{\text{f}}\} \mathbb{P}\{U_{\text{f}} = i\}. \tag{14}$$

C. Coverage Probability

The coverage probability is the complementary cumulative distribution function (ccdf) of the SINR, $P_{\text{c}}(\theta) = \mathbb{P}(\text{SINR} > \theta)$, where θ is the SINR threshold. In deriving the coverage probabilities in the following, we make use of an independent thinning approximation; that is, for each sub-band, the event that it is used by an MBS is independent of the event that it is used by all the other MBSs. Such an approximation essentially neglects the fact that the areas of adjacent Poisson Voronoi cells are spatially correlated, and thus tends to underestimate the inter-cell interference; however, our numerical study has found that the discrepancy between this approximation (along with others) and simulation experiments is rather slight (also see, e.g., [9]).

1) Orthogonal Spectrum Allocation:

Theorem 1: The coverage probability of a UE connected to its serving MBS is given by

$$P_{\text{c}}^{\text{m},\perp}(\theta) = \int_0^{\infty} \pi \lambda_{\text{m}}^{\text{BS}} e^{-\pi v(\lambda_{\text{m}}^{\text{BS}} + \tilde{\lambda}_{\text{m}}^{\text{BS}} \rho(\theta,\alpha)) - \frac{\theta v^{1/\delta} \sigma^2}{P_{\text{m}}}} \mathrm{d}v. \tag{15}$$

The coverage probability of a UE connected to its serving FAP is given by

$$P_{\text{c}}^{\text{f},\perp}(\theta) = \int_0^{R_{\text{f}}^2} \frac{1}{R_{\text{f}}^2} e^{-\frac{\theta v^{1/\delta} \sigma^2}{P_{\text{f}}} - \tilde{\lambda}_{\text{f}}^{\text{BS}} v \theta^{\delta} \delta \pi^2 \csc(\delta\pi)} \mathrm{d}v, \tag{16}$$

where $\delta = 2/\alpha$, $\tilde{\lambda}_{\text{m}}^{\text{BS}} = \lambda_{\text{m}}^{\text{BS}} P_{\text{busy}}^{\text{m},\perp}$, $\tilde{\lambda}_{\text{f}}^{\text{BS}} = \lambda_{\text{f}}^{\text{BS}} P_{\text{busy}}^{\text{f},\perp}$, and $\rho(\theta,\alpha) = \theta^{\delta} \int_{\theta^{-\delta}}^{\infty} \frac{1}{1+x^{1/\delta}} \mathrm{d}x$.

Proof: See Appendix A.

2) Non-orthogonal Spectrum Allocation:

Theorem 2: The coverage probability of a UE connected to its serving MBS is given by

$$\begin{aligned} P_{\text{c}}^{\text{m},\not\perp}(\theta) = \int_0^{\infty} \pi \lambda_{\text{m}}^{\text{BS}} \exp\Big(& -\pi v(\lambda_{\text{m}}^{\text{BS}} + \tilde{\lambda}_{\text{m}}^{\text{BS}} \rho(\theta,\alpha)) \\ & - \frac{\theta v^{1/\delta} \sigma^2}{P_{\text{m}}} - v \tilde{\lambda}_{\text{f}}^{\text{BS}} \left(\frac{P_{\text{f}} \theta}{P_{\text{m}}}\right)^{\delta} \delta \pi^2 \csc(\delta\pi) \Big) \mathrm{d}v. \end{aligned} \tag{17}$$

The coverage probability of a UE connected to its serving FAP is given by

$$\begin{aligned} & P_{\text{c}}^{\text{f},\not\perp}(\theta) = \\ & \int_0^{R_{\text{f}}^2} \frac{1}{R_{\text{f}}^2} e^{-\frac{\theta v^{1/\delta} \sigma^2}{P_{\text{f}}} - \delta \pi^2 \csc(\delta\pi) \theta^{\delta} v (\tilde{\lambda}_{\text{f}}^{\text{BS}} + \tilde{\lambda}_{\text{m}}^{\text{BS}} (\frac{P_{\text{m}}}{P_{\text{f}}})^{\delta})} \mathrm{d}v, \end{aligned} \tag{18}$$

where $\tilde{\lambda}_{\text{m}}^{\text{BS}} = \lambda_{\text{m}}^{\text{BS}} P_{\text{busy}}^{\text{m},\not\perp}$ and $\tilde{\lambda}_{\text{f}}^{\text{BS}} = \lambda_{\text{f}}^{\text{BS}} P_{\text{busy}}^{\text{f},\not\perp}$.

Proof: See Appendix B.

D. Data Rate

The instantaneous data rate that the sub-channel can accommodate is $R = W \log_2(1 + \text{SINR})$. The actually achieved data rates, after taking into consideration the UE load and sub-band occupancy, are given below. Without loss of generality, we take an MBS for example. When the number of UEs in a macro cell does not exceed the total number of sub-bands (i.e., $U_{\text{m}} \le N_{\text{m}}$), each UE can exclusively occupy a sub-band, and its data rate is denoted by R_{m}; when $U_{\text{m}} > N_{\text{m}}$, the U_{m} UEs need to share the N_{m} sub-bands, and the data rate is thus $\frac{N_{\text{m}}}{U_{\text{m}}} R_{\text{m}}$, assuming a round-robin sharing mechanism. So the data rate of a UE served by an MBS is given by

$$\begin{aligned} R_{\text{m}}^{\text{UE}} &= \xi_{\text{m}} R_{\text{m}}, \text{ with} \\ \xi_{\text{m}} &= \frac{\sum_{i=1}^{N_{\text{m}}} \mathbb{P}\{U_{\text{m}} = i\} + \sum_{N_{\text{m}}+1}^{\infty} \mathbb{P}\{U_{\text{m}} = i\} \frac{N_{\text{m}}}{i}}{1 - \mathbb{P}\{U_{\text{m}} = 0\}}. \end{aligned} \tag{19}$$

Similarly, the data rate of a UE served by an FAP is given by

$$\begin{aligned} R_{\text{f}}^{\text{UE}} &= \xi_{\text{f}} R_{\text{f}}, \text{ with} \\ \xi_{\text{f}} &= \frac{\sum_{i=1}^{N_{\text{f}}} \mathbb{P}\{U_{\text{f}} = i\} + \sum_{N_{\text{f}}+1}^{\infty} \mathbb{P}\{U_{\text{f}} = i\} \frac{N_{\text{f}}}{i}}{1 - \mathbb{P}\{U_{\text{f}} = 0\}}. \end{aligned} \tag{20}$$

IV. Standard-Definition Outage Probability and High-Definition Probability

In this section we evaluate the performance metrics, namely, the Standard-Definition outage probability and the High-Definition probability, of the model. The Standard-Definition outage probability provides a quantification of the proportion of UEs that cannot receive any content, while the High-Definition probability indicates the proportion of UEs that are able to receive high-quality content.

A. Decoupled Transmission

For a macro UE, only base layer is transmitted via its serving MBS, so the Standard-Definition outage probability $P_{\rm SD}^{\rm m}$ is

$$P_{\rm SD}^{\rm m} = \mathbb{P}\{R_{\rm m}^{\rm UE} < R_{\rm B}\} = 1 - P_{\rm c}^{{\rm m},s}\Big(2^{\frac{R_{\rm B}/\xi_{\rm m}}{W}}\Big), \qquad (21)$$

where the superscript $s \in \{\perp, \not\perp\}$ indicates whether the orthogonal or non-orthogonal spectrum allocation scheme is used (the same notation applies throughout this section).

For a femto UE, both the base layer and the enhancement layer are transmitted via its serving FAP, so the Standard-Definition outage probability $P_{\rm SD}^{\rm f}$ is

$$P_{\rm SD}^{\rm f} = \mathbb{P}\{R_{\rm f}^{\rm UE} < R_{\rm B}\} = 1 - P_{\rm c}^{{\rm f},s}\Big(2^{\frac{R_{\rm B}/\xi_{\rm f}}{W}}\Big), \qquad (22)$$

and the High-Definition probability $P_{\rm HD}^{\rm f}$ is

$$P_{\rm HD}^{\rm f} = \mathbb{P}\{R_{\rm f}^{\rm UE} > R_{\rm B} + R_{\rm E}\} = P_{\rm c}^{{\rm f},s}\Big(2^{\frac{(R_{\rm B}+R_{\rm E})/\xi_{\rm f}}{W}}\Big). \qquad (23)$$

B. Coupled Transmission

Since all the UEs connect to the macro tier for the base layer, the Standard-Definition outage probabilities $P_{\rm SD}^{\rm m}$ and $P_{\rm SD}^{\rm f}$ are the same for macro and femto UEs,

$$P_{\rm SD}^{\rm m} = P_{\rm SD}^{\rm f} = \mathbb{P}\{R_{\rm m}^{\rm UE} < R_{\rm B}\} = 1 - P_{\rm c}^{{\rm m},s}\Big(2^{\frac{R_{\rm B}/\xi_{\rm m}}{W}}\Big). \qquad (24)$$

For a femto UE, in the orthogonal case its connection to its serving MBS and that to its serving FAP are independent; in the non-orthogonal case, such an independence does not hold. In the following analysis, we make use of a tier independence approximation; that is, for a UE, its rate from the macro tier, $R_{\rm m}^{\rm UE}$, and its rate from the femto tier, $R_{\rm f}^{\rm UE}$, are independent r.v.s. Such an approximation is partially motivated by the randomized sub-band selection in the non-orthogonal spectrum allocation scheme and is found to be practically accurate via simulation experiments. By the tier independence approximation, the High-Definition probability for femto UEs denoted by $P_{\rm HD}^{\rm f}$ is

$$\begin{aligned} P_{\rm HD}^{\rm f} &= \mathbb{P}\{R_{\rm m}^{\rm UE} > R_{\rm B}, R_{\rm f}^{\rm UE} > R_{\rm E}\} \\ &= P_{\rm c}^{{\rm m},s}\Big(2^{\frac{R_{\rm B}/\xi_{\rm m}}{W}}\Big) P_{\rm c}^{{\rm f},s}\Big(2^{\frac{R_{\rm E}/\xi_{\rm f}}{W}}\Big). \end{aligned} \qquad (25)$$

C. Hybrid Transmission

For a macro UE, only the base layer is transmitted via its serving MBS, so the Standard-Definition outage probability $P_{\rm SD}^{\rm m}$ is

$$P_{\rm SD}^{\rm m} = \mathbb{P}\{R_{\rm m}^{\rm UE} < R_{\rm B}\} = 1 - P_{\rm c}^{{\rm m},s}\Big(2^{\frac{R_{\rm B}/\xi_{\rm m}}{W}}\Big). \qquad (26)$$

A femto UE either connects to its serving MBS with probability p or its serving FAP with probability $1-p$, so the Standard-Definition outage probability is

$$\begin{aligned} P_{\rm SD}^{\rm f} &= p\mathbb{P}\{R_{\rm m}^{\rm UE} < R_{\rm B}\} + (1-p)\mathbb{P}\{R_{\rm f}^{\rm UE} < R_{\rm B}\} \\ &= p\Big(1 - P_{\rm c}^{{\rm m},s}\Big(2^{\frac{R_{\rm B}/\xi_{\rm m}}{W}}\Big)\Big) \\ &\quad + (1-p)\Big(1 - P_{\rm c}^{{\rm f},s}\Big(2^{\frac{R_{\rm B}/\xi_{\rm f}}{W}}\Big)\Big). \end{aligned} \qquad (27)$$

By the tier independence approximation, the High-Definition probability of a femto UE is

$$\begin{aligned} P_{\rm HD}^{\rm f} &= p\mathbb{P}\{R_{\rm m}^{\rm UE} > R_{\rm B}\}\mathbb{P}\{R_{\rm f}^{\rm UE} > R_{\rm E}\} \\ &\quad + (1-p)\mathbb{P}\{R_{\rm f}^{\rm UE} > R_{\rm B} + R_{\rm E}\} \\ &= pP_{\rm c}^{{\rm m},s}\Big(2^{\frac{R_{\rm B}/\xi_{\rm m}}{W}}\Big) P_{\rm c}^{{\rm f},s}\Big(2^{\frac{R_{\rm E}/\xi_{\rm f}}{W}}\Big) \\ &\quad + (1-p)P_{\rm c}^{{\rm f},s}\Big(2^{\frac{(R_{\rm B}+R_{\rm E})/\xi_{\rm f}}{W}}\Big). \end{aligned} \qquad (28)$$

V. Interference Cancellation

In this section we consider an enhancement of femto UEs in the *Coupled Transmission* protocol, who connect to their serving MBSs for the base layer and to their serving FAPs for the enhancement layer. Under this scenario, the UE may employ Interference Cancellation (IC) to improve the performance.

Due to the advantage of interference cancellation, it is a viable option, for each femto UE, to let its base layer transmission from an MBS and its enhancement layer transmission from an FAP be on the same sub-band, thus saving spectrum resources. So here, we consider the following spectrum allocation scheme:
(1) A femto UE exclusively occupies a sub-band for its femto tier connection if $U_{\rm f} \le N$ or shares a sub-band with the other femto UEs subscribing to the same FAP otherwise;
(2) this femto UE occupies the same sub-band for its macro tier connection, either exclusively if $U_{\rm m} \le N$ or in a round-robin sharing fashion with the other UEs served by the same MBS otherwise.

The distributions of $U_{\rm f}$ and $U_{\rm m}$ are the same as those of *Coupled Transmission* in Section III-A1. The probability that a sub-band is used by an MBS (resp. an FAP) is

$$P_{\rm busy}^{\rm m,IC} = \frac{1}{N}\sum_{i=0}^{\infty} \min\{i, N\}\mathbb{P}\{U_{\rm m} = i\}, \qquad (29)$$

$$P_{\rm busy}^{\rm f,IC} = \frac{1}{N}\sum_{i=0}^{\infty} \min\{i, N\}\mathbb{P}\{U_{\rm f} = i\}. \qquad (30)$$

A femto UE first attempts to decode its enhancement layer transmitted from its serving FAP, and, if successful, it subtracts that part from its received signal from its serving MBS and then decodes its base layer. We have the following result.

Theorem 3: For a femto UE, denote the event that it decodes its enhancement layer as E_1 and the event that it decodes its base layer after interference cancellation as E_2. Then, $\mathbb{P}\{E_1\} = \mathbb{P}\{R_{\rm f}^{\rm UE} > R_{\rm E}\} = P_{\rm c}^{{\rm f},\not\perp}\Big(2^{\frac{R_{\rm E}/\xi_{\rm f}}{W}}\Big)$, and $\mathbb{P}\{E_1, E_2\}$ is given by (32), where $\tilde{\lambda}_{\rm m}^{\rm BS} = \lambda_{\rm m}^{\rm BS} P_{\rm busy}^{\rm m,IC}$ and $\tilde{\lambda}_{\rm f}^{\rm BS} = \lambda_{\rm f}^{\rm BS} P_{\rm busy}^{\rm f,IC}$.

Proof: See Appendix C.

For a macro UE, the Standard-Definition outage probability is not affected by interference cancellation, hence

$$P_{\rm SD}^{\rm m} = \mathbb{P}\{R_{\rm m}^{\rm UE} < R_{\rm B}\} = 1 - P_{\rm c}^{{\rm m},\not\perp}\Big(2^{\frac{R_{\rm B}/\xi_{\rm m}}{W}}\Big). \qquad (33)$$

For a femto UE, the Standard-Definition outage probability $P_{\rm SD}^{\rm f}$ and the High-Definition probability $P_{\rm HD}^{\rm f}$ are

$$P_{\rm SD}^{\rm f} = \mathbb{P}\{E_1\} - \mathbb{P}\{E_1, E_2\} + P_{\rm SD}^{\rm m}(1 - \mathbb{P}\{E_1\}), \qquad (34)$$

$$P_{\rm HD}^{\rm f} = \mathbb{P}\{E_1, E_2\}. \qquad (35)$$

$$\mathbb{P}\{E_1, E_2\} = \int_0^\infty 2\pi\lambda_{\rm m}^{\rm BS} r_{\rm m} e^{-\lambda_{\rm m}^{\rm BS}\pi r_{\rm m}^2} \int_0^{R_{\rm f}} \frac{2r_{\rm f}}{R_{\rm f}^2} \Big(e^{-\sigma^2 \frac{\theta_{\rm m} r_{\rm m}^\alpha}{P_{\rm m}} - \pi\tilde{\lambda}_{\rm m}^{\rm BS} r_{\rm m}^2 \rho(\theta_{\rm m},\alpha) - \pi\tilde{\lambda}_{\rm f}^{\rm BS} r_{\rm f}^2 \rho\left(\frac{\theta_{\rm m} r_{\rm m}^\alpha P_{\rm f}}{r_{\rm f}^\alpha P_{\rm m}},\alpha\right)}$$
$$- \frac{1}{\frac{r_{\rm m}^\alpha P_{\rm f}}{r_{\rm f}^\alpha P_{\rm m}\theta_{\rm f}} + 1} e^{-\delta^2\left(\frac{r_{\rm m}^\alpha\theta_{\rm m}}{P_{\rm m}} + (1+\theta_{\rm m})\frac{\theta_{\rm f} r_{\rm f}^\alpha}{P_{\rm f}}\right) - \pi\tilde{\lambda}_{\rm m}^{\rm BS} r_{\rm m}^2 \rho\left(\theta_{\rm m} + \frac{\theta_{\rm f} r_{\rm f}^\alpha P_{\rm m}(1+\theta_{\rm m})}{P_{\rm f} r_{\rm m}^\alpha},\alpha\right) - \pi\tilde{\lambda}_{\rm f}^{\rm BS} r_{\rm f}^2 \rho\left(\frac{r_{\rm m}^\alpha P_{\rm f}}{r_{\rm f}^\alpha P_{\rm m}} + \theta_{\rm f}(1+\theta_{\rm m}),\alpha\right)} \Big) {\rm d}r_{\rm f}{\rm d}r_{\rm m}. \quad (32)$$

TABLE I
SYSTEM PARAMETERS

Symbol	Description	Value
N	number of sub-bands	20
W	bandwidth of a sub-band (MHz)	2
$P_{\rm m}$	MBS transmit power per sub-band (dBm)	39
$P_{\rm f}$	FAP transmit power per sub-band (dBm)	13
σ^2	noise power (dBm)	-104
$\lambda_{\rm m}^{\rm BS}$	MBS intensity ($\rm m^{-2}$)	1E-5
$\lambda_{\rm f}^{\rm BS}$	FAP intensity ($\rm m^{-2}$)	5E-5
$\lambda_{\rm m}^{\rm UE}$	macro UE intensity ($\rm m^{-2}$)	2E-4
$\lambda_{\rm f}^{\rm UE}$	femto UE intensity in coverage ($\rm m^{-2}$)	8E-3
$R_{\rm f}$	coverage radius of FAP (m)	20
α	path loss exponent	4
$R_{\rm B}$	rate for basic layer transmission	100kbps
$R_{\rm E}$	rate for enhancement layer transmission [3]	900kbps

VI. NUMERICAL ILLUSTRATION

In this section, the Standard-Definition outage probabilities and the High-Definition probabilities are evaluated for the transmission protocols considered under orthogonal and non-orthogonal spectrum allocation schemes. Unless otherwise specified, the system parameters are listed in Table I.

Fig. 2(a) displays the performance in the orthogonal case. In that case, $N_{\rm m}$ sub-bands for the macro tier and $N_{\rm f}$ sub-bands for the femto tier are orthogonal, and $N_{\rm m} + N_{\rm f} = N$. As $N_{\rm m}$ increases, more resources are allocated to the macro tier, and the Standard-Definition outage probabilities decrease for both macro UEs and femto UEs, under all transmission protocols, except that the femto UE Standard-Definition outage probabilities slightly increase for very large values of $N_{\rm m}$. The High-Definition probability under *Decoupled Transmission* decreases with $N_{\rm m}$ because the transmission of enhancement layer via FAPs deteriorates as the resources for the femto tier are reduced. The High-Definition probabilities for *Coupled Transmission* and *Hybrid Transmission* increase for small $N_{\rm m}$ and then decrease as $N_{\rm m}$ grows large, reflecting the tension between the resources for base layer transmission and enhancement layer transmission.

Fig. 2(b) displays the performance in the non-orthogonal case. Here for comparison with Fig. 2(a), we let $N_{\rm m}+N_{\rm f} = N$, whereas we note that the $N_{\rm m}$ sub-bands for the macro tier and $N_{\rm f}$ sub-bands for the femto tier are not orthogonal, but are randomly selected by each BS independently. The general trend is largely similar to that in the orthogonal case, but the difference lies in

[3]For example [10], we consider two spatial resolutions at QQVGA and QVGA, two temporal layers of 25fps and 12.5fps, and two quality layers with lowest/highest target rate. $R_{\rm B}$ is about 100 kbps, and $R_{\rm E}$ is about 900 kbps.

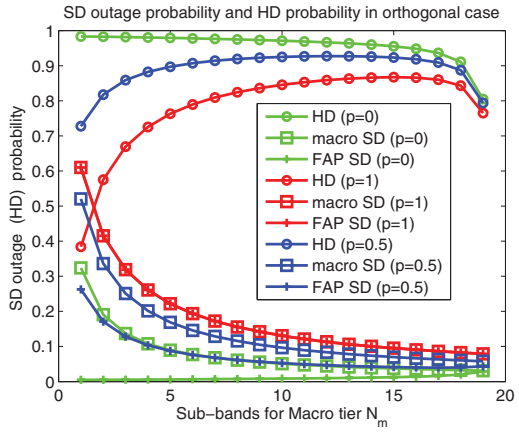

(a)

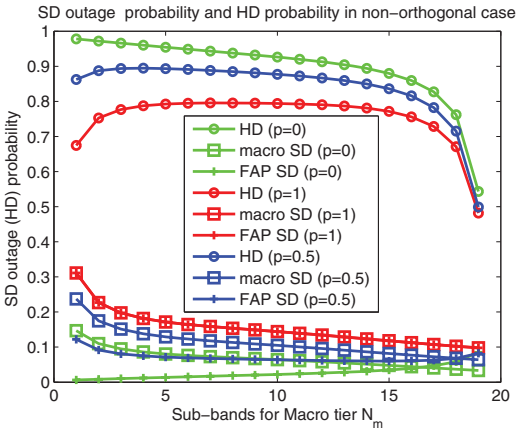

(b)

Fig. 2. Performance illustration: $p = 0$ denotes *Decoupled Transmission*, $p = 1$ denotes *Coupled Transmission*, and $p = 0.5$ denotes *Hybrid Transmission*. Note that for *Coupled Transmission* the macro Standard-Definition outage probability and the femto Standard-Definition outage probability are the same.

that the curves show less variability with $N_{\rm m}$ (except for those near to N), compared with the orthogonal case. The reason for such a practically desirable insensitivity is due to the lessened tension between the resources for macro tiers and femto tiers, from randomized sub-band selection.

In both orthogonal and non-orthogonal cases, the performance of *Decoupled Transmission* is the best and that of *Coupled Transmission* is the worst. But from an implementation perspective, *Coupled Transmission* has the advantage that it enables a UE to receive the base layer from the macro tier uninterruptedly,

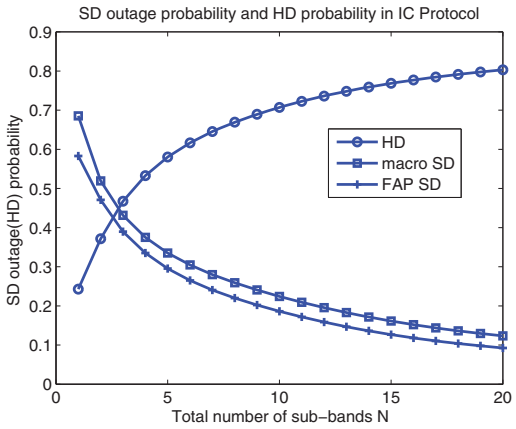

Fig. 3. Performance of interference cancellation.

thus maintaining a smooth transition in roaming and reducing handover cost between tiers.

As displayed in Fig. 3, the performance of *Coupled Transmission* can be further improved by interference cancellation described in Section V. Here the number of sub-bands, N, is not fixed but increasing from one to twenty. As N increases, both the macro and femto Standard-Definition outage probabilities decrease, and the High-Definition probability increases. When $N = 20$, the achieved tradeoff between the Standard-Definition outage probability and the High-Definition probability is superior to that achieved by any choice of N_{m} in Fig. 2(a) and Fig. 2(b).

VII. Conclusion

We considered transmitting layered source information, such as SVC, over tiered cellular networks, aiming at providing High-Definition content for UEs subscribed to femto tier services, while maintaining acceptable basic transmission quality for regular UEs. We proposed several transmission protocols and analyzed their performance metrics. We observe that the proposed framework of scalable transmission over heterogenous networks is an effective means for providing differentiated services for users.

Acknowledgements

The research of L. Wu, Y. Zhong and W. Zhang has been supported by National Basic Research Program of China (973 Program) through grant 2012CB316004 and National Natural Science Foundation of China through grant 61379003; the research of M. Haenggi has been supported by the U.S. National Science Foundation through grant CCF 1216407.

Appendix A

Let l_{m} be the distance between a macro UE and its serving MBS, which is the nearest MBS. So the pdf of l_{m} is

$$f_{l_{\mathrm{m}}}(r) = e^{-\lambda_{\mathrm{m}}^{\mathrm{BS}}\pi r^2} 2\pi\lambda_{\mathrm{m}}^{\mathrm{BS}} r. \tag{36}$$

Under orthogonal spectrum allocating scheme, the SINR experienced by the macro UE is given by $\mathrm{SINR} = \frac{P_{\mathrm{m}} h_{b_0} l_{\mathrm{m}}^{-\alpha}}{I_{\mathrm{m}}+\sigma^2}$, where $I_{\mathrm{m}} = \sum_{x\in\Phi'_{\mathrm{m}}\setminus\{b_0\}} P_{\mathrm{m}} h_x \|x\|^{-\alpha}$ is the interference from the macro tier (excluding the serving MBS itself which is denoted by b_0). Due to the independent thinning approximation, the set of interfering MBSs is a PPP Φ'_{m} with intensity $\tilde{\lambda}_{\mathrm{m}}^{\mathrm{BS}}$. The ccdf of the SINR of a macro UE is thus

$$\begin{aligned} P_{\mathrm{c}}^{\mathrm{m},\perp}(\theta) &= \mathbb{P}\{\mathrm{SINR} > \theta\} \\ &= \int_0^\infty 2\pi\lambda_{\mathrm{m}}^{\mathrm{BS}} r e^{-\pi\lambda_{\mathrm{m}}^{\mathrm{BS}} r^2} \mathbb{P}\left\{\frac{P_{\mathrm{m}} h_{b_0} r^{-\alpha}}{I_{\mathrm{m}}+\sigma^2} > \theta\right\} \mathrm{d}r \\ &\overset{(a)}{=} \int_0^\infty 2\pi\lambda_{\mathrm{m}}^{\mathrm{BS}} r e^{-\pi\lambda_{\mathrm{m}}^{\mathrm{BS}} r^2 - \frac{\theta r^\alpha \sigma^2}{P_{\mathrm{m}}}} \mathcal{L}_{I_{\mathrm{m}}}\left(\frac{\theta r^\alpha}{P_{\mathrm{m}}}\right) \mathrm{d}r, \end{aligned} \tag{37}$$

where (a) follows from $h_{b_0} \sim \mathrm{Exp}(1)$.

Applying the pgfl of PPP yields

$$\begin{aligned} \mathcal{L}_{I_{\mathrm{m}}}(s) &= \exp\left(-2\pi\tilde{\lambda}_{\mathrm{m}}^{\mathrm{BS}} \int_r^\infty (1 - \frac{1}{1+sP_{\mathrm{m}}x^{-\alpha}}) x\mathrm{d}x\right) \\ &= e^{-\pi\tilde{\lambda}_{\mathrm{m}}^{\mathrm{BS}} r^2 \rho(\frac{sP_{\mathrm{m}}}{r^\alpha},\alpha)}, \end{aligned} \tag{38}$$

which, when substituted into $P_{\mathrm{c}}^{\mathrm{m},\perp}(\theta)$, leads to (15).

Let l_{f} be the distance between a femto UE and its serving FAP. Since femto UEs are uniformly distributed in the circular coverage area of radius R_{f} of each FAP, the pdf of l_{f} is given by $f_{l_{\mathrm{f}}}(r) = \frac{2r}{R_{\mathrm{f}}^2}$. The ccdf of the SINR of a femto UE can then be derived in an analogous way as that of $P_{\mathrm{c}}^{\mathrm{m},\perp}(\theta)$ above,

$$\begin{aligned} P_{\mathrm{c}}^{\mathrm{f},\perp}(\theta) &= \mathbb{P}\{\mathrm{SINR} > \theta\} \\ &= \int_0^{R_{\mathrm{f}}} \frac{2r}{R_{\mathrm{f}}^2} e^{\frac{-\theta r^\alpha \delta^2}{P_{\mathrm{f}}}} \mathcal{L}_{I_{\mathrm{f}}}(\frac{\theta r^\alpha}{P_{\mathrm{f}}}) \mathrm{d}r, \end{aligned} \tag{39}$$

which, after expanding the Laplace transform of I_{f} and further manipulations, leads to (16).

Appendix B

Since there is inter-tier interference in the non-orthogonal spectrum allocating scheme, the SINR experienced by a macro UE is given by $\mathrm{SINR} = \frac{P_{\mathrm{m}} h_{b_0} l_{\mathrm{m}}^{-\alpha}}{I_{\mathrm{m}}+I_{\mathrm{f}}+\sigma^2}$, where $I_{\mathrm{m}} = \sum_{x\in\Phi'_{\mathrm{m}}\setminus\{b_0\}} P_{\mathrm{m}} h_x \|x\|^{-\alpha}$ is the interference from the macro tier (excluding the serving MBS itself which is denoted by b_0), and $I_{\mathrm{f}} = \sum_{x\in\Phi_{\mathrm{f}}} P_{\mathrm{f}} h_x \|x\|^{-\alpha}$ is the interference from the femto tier. The set of interfering MBSs is a PPP Φ'_{m} with intensity $\tilde{\lambda}_{\mathrm{m}}^{\mathrm{BS}}$, and the set of interfering FAPs is a PPP Φ'_{f} with intensity $\tilde{\lambda}_{\mathrm{f}}^{\mathrm{BS}}$. Thus

$$\begin{aligned} P_{\mathrm{c}}^{\mathrm{m},\not\perp}(\theta) &= \mathbb{P}\{\mathrm{SINR} > \theta\} \\ &= \int_0^\infty 2\pi\lambda_{\mathrm{m}}^{\mathrm{BS}} r e^{-\pi\lambda_{\mathrm{m}}^{\mathrm{BS}} r^2} \mathbb{P}\left\{\frac{P_{\mathrm{m}} h_{b_0} r^{-\alpha}}{I_{\mathrm{m}}+I_{\mathrm{f}}+\sigma^2} > \theta\right\} \mathrm{d}r \\ &= \int_0^\infty 2\pi\lambda_{\mathrm{m}}^{\mathrm{BS}} r e^{-\pi\lambda_{\mathrm{m}}^{\mathrm{BS}} r^2 - \frac{\theta r^\alpha \sigma^2}{P_{\mathrm{m}}}} \mathcal{L}_{I_{\mathrm{m}}+I_{\mathrm{f}}}\left(\frac{\theta r^\alpha}{P_{\mathrm{m}}}\right) \mathrm{d}r \end{aligned} \tag{40}$$

The Laplace transform of I_{f} is

$$\begin{aligned} \mathcal{L}_{I_{\mathrm{f}}}(s) &= \exp\left(-2\pi\tilde{\lambda}_{\mathrm{f}}^{\mathrm{BS}} \int_0^\infty \left(1 - \frac{1}{1+sP_{\mathrm{f}}x^{-\alpha}}\right) x\mathrm{d}x\right) \\ &= e^{-\delta\pi^2 \csc(\delta\pi)\tilde{\lambda}_{\mathrm{f}}^{\mathrm{BS}}(sP_{\mathrm{f}})^\delta}. \end{aligned} \tag{41}$$

Substituting (38) and (41) into $P_{\mathrm{c}}^{\mathrm{m},\not\perp}(\theta)$, we obtain (17).

Similar to the derivation of $P_{\mathrm{c}}^{\mathrm{m},\not\perp}(\theta)$, by swapping the role of macro tier and femto tier, we can evaluate the SINR distribution experienced by a femto UE, and obtain $P_{\mathrm{c}}^{\mathrm{f},\not\perp}(\theta)$ in (18).

APPENDIX C

The SINR of the link from an FAP to its served UE is $\frac{P_{\rm f} h_{b_0^{\rm f}} l_{\rm f}^{-\alpha}}{I_{\rm m}+I_{\rm f}+I_{\rm m0}+\sigma^2}$, and the SINR of the link from an MBS to its served UE is $\frac{P_{\rm m} h_{b_0^{\rm m}} l_{\rm m}^{-\alpha}}{I_{\rm m}+I_{\rm f}+\sigma^2}$, where $I_{\rm m}=\sum_{x\in\Phi'_{\rm m}\setminus\{b_0^{\rm m}\}} P_{\rm m} h_x \|x\|^{-\alpha}$ (excluding the serving MBS itself which is denoted by $b_0^{\rm m}$) is the interference from the macrocell tier, $I_{\rm m0} = P_{\rm m} h_{b_0^{\rm m}} l_{\rm m}^{-\alpha}$ denotes the interference from the nearest MBS, $I_{\rm f}=\sum_{x\in\Phi'_{\rm f}\setminus\{b_0^{\rm f}\}} P_{\rm f} h_x \|x\|^{-\alpha}$ is the interference from the femtocell tier (excluding the serving FAP itself which is denoted by $b_0^{\rm f}$). $\theta_{\rm m}$ and $\theta_{\rm f}$ denote the SINR threshold for the correct reception of base layer and enhancement layer respectively.

$$\begin{aligned}
\mathbb{P}\{E_1,E_2\} &= \mathbb{P}\Big(\frac{P_{\rm m} h_{b_0^{\rm m}} l_{\rm m}^{-\alpha}}{I_{\rm m}+I_{\rm f}+\sigma^2} > \theta_{\rm m}, \\
&\qquad \frac{P_{\rm f} h_{b_0^{\rm f}} l_{\rm f}^{-\alpha}}{I_{\rm m}+I_{\rm f}+I_{\rm m0}+\sigma^2} > \theta_{\rm f}\Big) \\
&= \mathbb{P}\Big(\underbrace{P_{\rm m} h_{b_0^{\rm m}} l_{\rm m}^{-\alpha}}_{Y} > \underbrace{\theta_{\rm m}(I_{\rm m}+I_{\rm f}+\sigma^2)}_{X}, \\
&\qquad P_{\rm m} h_{b_0^{\rm m}} l_{\rm m}^{-\alpha} < \underbrace{\frac{P_{\rm f} h_{b_0^{\rm f}} l_{\rm f}^{-\alpha}}{\theta_{\rm f}} - I_{\rm m} - I_{\rm f} - \sigma^2}_{Z}\Big) \\
&= \mathbb{E}_{I_{\rm m},I_{\rm f},l_{\rm m},l_{\rm f},h_{b_0^{\rm f}}}\{\mathbb{P}(Y>X, Y<Z | I_{\rm m}, I_{\rm f}, l_{\rm m}, l_{\rm f}, h_{b_0^{\rm f}})\} \\
&\overset{(a)}{=} \mathbb{E}_{I_{\rm m},I_{\rm f},l_{\rm m},l_{\rm f}}\Big\{ e^{-\frac{\theta_{\rm m} l_{\rm m}^{\alpha}}{P_{\rm m}}(I_{\rm m}+I_{\rm f}+\sigma^2)} \\
&\qquad - \frac{1}{\frac{l_{\rm m}^{\alpha} P_{\rm f}}{l_{\rm f}^{\alpha} P_{\rm m} \theta_{\rm f}}+1} e^{-(I_{\rm m}+I_{\rm f}+\delta^2)\left(\frac{l_{\rm m}^{\alpha}}{P_{\rm m}}+(1+\theta_{\rm m})\frac{\theta_{\rm f} l_{\rm f}^{\alpha}}{P_{\rm f}}\right)} \Big\} \\
&= \mathbb{E}_{l_{\rm m},l_{\rm f}}\Big\{ e^{-\sigma^2 \frac{\theta_{\rm m} l_{\rm m}^{\alpha}}{P_{\rm m}}} \mathcal{L}_{I_{\rm m}+I_{\rm f}}\Big(\frac{\theta_{\rm m} l_{\rm m}^{\alpha}}{P_{\rm m}}\Big) \\
&\qquad - \frac{1}{\frac{l_{\rm m}^{\alpha} P_{\rm f}}{l_{\rm f}^{\alpha} P_{\rm m} \theta_{\rm f}}+1} e^{-\delta^2\left(\frac{l_{\rm m}^{\alpha}}{P_{\rm m}}+(1+\theta_{\rm m})\frac{\theta_{\rm f} l_{\rm f}^{\alpha}}{P_{\rm f}}\right)} \\
&\qquad \times \mathcal{L}_{I_{\rm m}+I_{\rm f}}\Big(\frac{l_{\rm m}^{\alpha}}{P_{\rm m}} + (1+\theta_{\rm m})\frac{\theta_{\rm f} l_{\rm f}^{\alpha}}{P_{\rm f}}\Big)\Big\} \\
&\overset{(b)}{=} \mathbb{E}_{l_{\rm m},l_{\rm f}}\Big\{ e^{A} - \frac{1}{\frac{l_{\rm m}^{\alpha} P_{\rm f}}{l_{\rm f}^{\alpha} P_{\rm m} \theta_{\rm f}}+1} e^{B}\Big\} \\
&\overset{(c)}{=} \int_0^{\infty} 2\pi\lambda_{\rm m}^{\rm BS} r_{\rm m} e^{-\lambda_{\rm m}^{\rm BS}\pi r_{\rm m}^2} \\
&\qquad \int_0^{R_{\rm f}} \frac{2 r_{\rm f}}{R_{\rm f}^2}\Big(e^{A} - \frac{1}{\frac{r_{\rm m}^{\alpha} P_{\rm f}}{r_{\rm f}^{\alpha} P_{\rm m} \theta_{\rm f}}+1} e^{B}\Big) {\rm d}r_{\rm f} {\rm d}r_{\rm m}, \qquad (42)
\end{aligned}$$

with

$$\begin{aligned}
A &= -\sigma^2 \frac{\theta_{\rm m} l_{\rm m}^{\alpha}}{P_{\rm m}} - \pi\tilde{\lambda}_{\rm m}^{\rm BS} l_{\rm m}^2 \rho(\theta_{\rm m},\alpha) - \pi\tilde{\lambda}_{\rm f}^{\rm BS} l_{\rm f}^2 \rho\Big(\frac{\theta_{\rm m} l_{\rm m}^{\alpha} P_{\rm f}}{l_{\rm f}^{\alpha} P_{\rm m}},\alpha\Big) \\
B &= -\delta^2\Big(\frac{l_{\rm m}^{\alpha}\theta_{\rm m}}{P_{\rm m}} + (1+\theta_{\rm m})\frac{\theta_{\rm f} l_{\rm f}^{\alpha}}{P_{\rm f}}\Big) \\
&\qquad - \pi\tilde{\lambda}_{\rm m}^{\rm BS} l_{\rm m}^2 \rho\Big(\theta_{\rm m} + \frac{\theta_{\rm f} l_{\rm f}^{\alpha} P_{\rm m}(1+\theta_{\rm m})}{P_{\rm f} l_{\rm m}^{\alpha}},\alpha\Big) \\
&\qquad - \pi\tilde{\lambda}_{\rm f}^{\rm BS} l_{\rm f}^2 \rho\Big(\frac{l_{\rm m}^{\alpha} P_{\rm f}}{l_{\rm f}^{\alpha} P_{\rm m}} + \theta_{\rm f}(1+\theta_{\rm m}),\alpha\Big), \qquad (43)
\end{aligned}$$

where (a) follows from

$$\begin{aligned}
&\mathbb{E}_{h_{b_0^{\rm f}}}\{\mathbb{P}(Y>X, Y<Z)|h_{b_0^{\rm f}}\} \\
&= \int_{\psi>C} \mathbb{P}\Big(\frac{\theta_{\rm m} l_{\rm m}^{\alpha}}{P_{\rm m}}(I_{\rm m}+I_{\rm f}+\sigma^2) < h_{b_0^{\rm m}} \\
&\qquad < \frac{l_{\rm m}^{\alpha}}{P_{\rm m}}\Big(\frac{P_{\rm f}\psi l_{\rm f}^{-\alpha}}{\theta_{\rm f}} - I_{\rm m} - I_{\rm f} - \sigma^2\Big)\Big) {\rm f}_{h_{b_0^{\rm f}}}(\psi){\rm d}\psi \\
&\overset{(d)}{=} \int_{\psi>C} \Big(e^{-\frac{\theta_{\rm m} l_{\rm m}^{\alpha}}{P_{\rm m}}(I_{\rm m}+I_{\rm f}+\sigma^2)} \\
&\qquad - e^{-\frac{l_{\rm m}^{\alpha}}{P_{\rm m}}\left(\frac{P_{\rm f}\psi l_{\rm f}^{-\alpha}}{\theta_{\rm f}} - I_{\rm m} - I_{\rm f} - \sigma^2\right)}\Big) {\rm f}_{h_{b_0^{\rm f}}}(\psi){\rm d}\psi \\
&\overset{(e)}{=} e^{-\frac{\theta_{\rm m} l_{\rm m}^{\alpha}}{P_{\rm m}}(I_{\rm m}+I_{\rm f}+\sigma^2)} \\
&\qquad - \frac{1}{\frac{l_{\rm m}^{\alpha} P_{\rm f}}{l_{\rm f}^{\alpha} P_{\rm m} \theta_{\rm f}}+1} e^{-(I_{\rm m}+I_{\rm f}+\delta^2)\left(\frac{l_{\rm m}^{\alpha}}{P_{\rm m}}+(1+\theta_{\rm m})\frac{\theta_{\rm f} l_{\rm f}^{\alpha}}{P_{\rm f}}\right)};
\end{aligned}$$

(b) follows from $\mathcal{L}_{I_{\rm m}}(s) = e^{-\pi\tilde{\lambda}_{\rm m}^{\rm BS} l_{\rm m}^2 \rho(\frac{s P_{\rm m}}{l_{\rm m}^{\alpha}},\alpha)}$ and $\mathcal{L}_{I_{\rm f}}(s) = e^{-\pi\tilde{\lambda}_{\rm f}^{\rm BS} l_{\rm f}^2 \rho(\frac{s P_{\rm f}}{l_{\rm f}^{\alpha}},\alpha)}$; (c) follows from the pdf of $l_{\rm m}$ as $f_{l_{\rm m}}(r_{\rm m}) = e^{-\lambda_{\rm m}^{\rm BS}\pi r_{\rm m}^2} 2\pi\lambda_{\rm m}^{\rm BS} r_{\rm m}$ and the pdf of $l_{\rm f}$ as $f_{l_{\rm f}}(r_{\rm f}) = \frac{2 r_{\rm f}}{R_{\rm f}^2}$; (d) and (e) follow from the fact the pdf of $h_{b_0^{\rm m}}$ and $h_{b_0^{\rm f}}$ are both exponential with mean $\mu=1$ and $C = (1+\theta_{\rm m})(I_{\rm m}+I_{\rm f}+\delta^2)\frac{\theta_{\rm f}}{P_{\rm f}} l_{\rm f}^{\alpha}$.

REFERENCES

[1] W. Li, "Overview of fine granularity scalability in MPEG-4 video standard," *IEEE Trans. Circuits and Systems for Video Technology*, vol. 11, no. 3, pp. 301–317, 2001.

[2] V. Chandrasekhar, J. G. Andrews, and A. Gatherer, "Femtocell networks: a survey," *IEEE Commun. Magazine*, vol. 46, no. 9, pp. 59–67, 2008.

[3] T. Schierl, T. Stockhammer, and T. Wiegand, "Mobile video transmission using scalable video coding," *IEEE Trans. Circuits and Systems for Video Technology*, vol. 17, no. 9, pp. 1204–1217, 2007.

[4] R. Radhakrishnan and A. Nayak, "An efficient video adaptation scheme for SVC transport over LTE networks," in *Proc. IEEE Int. Conf. Parallel and Distributed Systems (ICPADS)*, 2011, pp. 127–133.

[5] V. Gupta, S. Somayazulu, N. Himayat, H. Verma, M. Bisht, and V. Nandwani, "Design challenges in transmitting scalable video over multi-radio networks," in *Proc. IEEE Globecom Workshops*, 2012, pp. 46–51.

[6] P. Konstantinos and I. George, "Video delivery over heterogeneous cellular networks: Optimizing cost and performance," in *Proc. IEEE INFOCOM*, 2014, pp. 1078–1086.

[7] M. Haenggi, *Stochastic Geometry for Wireless Networks*, Cambridge University Press, 2012.

[8] J.-S. Ferenc and Z. Néda, "On the size distribution of Poisson Voronoi cells," *Physica A: Statistical Mechanics and its Applications*, vol. 385, no. 2, pp. 518–526, 2007.

[9] Y. Zhong and W. Zhang, "Multi-channel hybrid access femtocells: a stochastic geometric analysis," *IEEE Trans. Commun.*, vol. 61, no. 7, pp. 3016-3026, 2013.

[10] A. Eichhorn and P. Ni, "Pick your layers wisely – a quality assessment of H.264 scalable video coding for mobile devices," in *Proc. IEEE Int. Conf. Commun.*, 2009, pp. 1–6.